Appl Phys A (2011) 105:555–563
DOI 10.1007/s00339-011-6598-3

Applied Physics A
Materials Science & Processing

RIR-MAPLE deposition of conjugated polymers for application to optoelectronic devices

Ryan Pate · Ryan McCormick · Li Chen · Weidong Zhou · Adrienne D. Stiff-Roberts

Received: 15 June 2011 / Accepted: 20 August 2011 / Published online: 24 September 2011
© Springer-Verlag 2011

Abstract Resonant-infrared matrix-assisted pulsed laser evaporation (RIR-MAPLE) is a promising deposition technology for the fabrication of conjugated polymer-based optoelectronic devices for two primary reasons: (i) the ability to control film morphology, and (ii) the ability to deposit multi-layered heterostructures. This article reviews a variation of RIR-MAPLE that uses emulsified targets of organic solvents and water such that the incident laser wavelength (Er:YAG at 2.9 μm) is resonant with hydroxyl (O–H) bonds in the host matrix, which are absent from the guest material. The novelty of the approach lies in the fact that while most polymers of interest and many compatible solvents do not resonantly absorb the laser energy at 2.9 μm, the emulsion with water enables high-quality, thin-film deposition with minimal photochemical and structural degradation for almost any polymer of interest. In addition, the advantages of emulsion-based RIR-MAPLE for conjugated polymer-based optoelectronic devices are demonstrated by two important studies. First, conjugated polymer films deposited by RIR-MAPLE are shown to have higher hole drift mobilities than films deposited using traditional drop-casting and spin-casting techniques. Second, the unique capability of RIR-MAPLE to enable conjugated polymer-based optical heterostructures is demonstrated by the fabrication and characterization of a multi-layer, polymer distributed Bragg reflector.

R. Pate · R. McCormick · A.D. Stiff-Roberts (✉)
Department of Electrical and Computer Engineering, Duke University, Durham, NC 27708, USA
e-mail: adrienne.stiffroberts@duke.edu

L. Chen · W. Zhou
Department of Electrical Engineering, University of Texas, Arlington, TX 76019, USA

1 Introduction

Organic polymers are generally considered to be insulators; however, conjugated polymers with an alternating single- and double-bond configuration enable charge transport due to one-dimensional periodicity and the close interaction of the molecular orbitals of the constituent monomers [1, 2]. As a result, the highest occupied molecular orbital (HOMO) and lowest unoccupied molecular orbital (LUMO) levels of the monomers split into bands that mimic the valence and conduction bands, respectively, of inorganic semiconductors. A broad range of conjugated polymer-based optoelectronic devices are under investigation, including infrared photodetectors [3, 4], lasers [5], light emitting diodes (LEDs) [6, 7], and photovoltaics [8–11], primarily due to the potential to realize performance comparable to traditional inorganic devices but with the capability for novel deployment, such as flexible substrates [12]. Yet, a fundamental challenge facing conjugated polymer-based optoelectronics is the strong dependence of device performance on film morphology and the inherent inability to control said morphology by traditional, solution-based deposition techniques [13–16]. Such solution-based deposition includes drop-casting [17], Langmuir Blodgett deposition [18], ink-jet printing [19], spraying [20], and spin-casting [21]. While many devices have been demonstrated using these techniques, solvent-induced conformational defects, e.g. bends and twists of individual polymer chains, are difficult to control. As a result, the device performance is often inconsistent and leads to low yield. In addition, next-generation conjugated polymer-based optoelectronics will require multi-layer device architectures, which can be difficult to achieve using solution-based processing without complex chemistry to alter the solubility of constituent materials [13, 22]. Therefore, this work describes a novel,

resonant-infrared (RIR) matrix-assisted pulsed laser evaporation (MAPLE) technique that uses a unique, emulsion-based target in order to control the surface and internal thin-film morphologies of conjugated polymers and to enable multi-layer, conjugated polymer heterostructures.

MAPLE deposition was first demonstrated in 1999 at the Naval Research Laboratory for the thin-film deposition of organic films, and the process was initially thought to be purely evaporative, wherein the guest material was deposited onto the substrate exclusively while the host matrix was completely evaporated and pumped away [23]. Later theoretical investigations indicated that MAPLE is more likely an ablative process, wherein both the guest material and host matrix are deposited onto the substrate because the host matrix is not completely evaporated [24–27]. The ablative nature of MAPLE deposition is particularly true for polymers due to the tendency of the polymer to leave the target as a polymer chain aggregate with significant solvent contamination [24–26]. Yet, it is important to note that this theory assumes an ultraviolet (UV) laser source for MAPLE deposition. Many studies of UV-MAPLE deposition use 193 nm or 248 nm lasers, the energy of which is absorbed by both the host matrix and the guest polymer in a target [26–29]. Therefore, such UV-MAPLE deposition is ablative, and the deposited films often demonstrate photochemical degradation, as determined by Fourier transform infrared (FTIR) absorbance measurements [23, 28, 30]. By using low concentrations of the guest polymer relative to the host matrix, photochemical degradation can be reduced, but is still persistent [28]. RIR-MAPLE is an attempt to achieve more evaporative deposition by mitigating the absorption of laser energy in the guest polymer by tuning an infrared laser to a specific absorption peak in the host matrix [28, 31]. Toftmann et al. used a free-electron laser at 8.2 μm to perform RIR-MAPLE deposition of a conjugated polymer by specifically targeting the long infrared absorption peak of the chloroform host matrix [28]. RIR-MAPLE using an Er:YAG laser at 2.9 μm, which is generally more accessible than free-electron lasers, was first used to deposit sorbent oligimers by targeting the hydroxyl (O–H) bond in a water matrix [31]. For both demonstrations of RIR-MAPLE, photochemical degradation of the deposited films was minimal. Thus, MAPLE deposition is most successful when the ideal laser-target interaction can be achieved, that is, evaporative deposition occurs when the incident laser energy is resonant with an absorption peak in the host matrix that is absent from the guest material. With regard to conjugated polymer deposition by RIR-MAPLE, the use of the more readily available Er:YAG laser was not pursued initially, primarily because the laser energy is not resonant with the majority of compatible solvents.

Accordingly, this work reviews a new RIR-MAPLE deposition technique that has been developed [32–35], wherein the ideal growth regime, i.e., strong laser absorption by the host matrix and little to no laser absorption by the guest material, can be achieved for almost any polymer. This important development is achieved by using an emulsified target matrix of organic solvents and water. The hydroxyl bond present in water (and ice, when frozen) is directly resonant with a 2.9-μm, Er:YAG laser source. The novelty of the approach lies in the fact that while most polymers of interest and many compatible solvents do not resonantly absorb the laser energy at 2.9 μm, the emulsion with water enables high-quality thin-film deposition with minimal photochemical and structural degradation for almost any polymer of interest. Further, the hydroxyl bond (O–H bond) concentration can be tuned by the target matrix chemistry such that the surface and internal morphologies of polymer thin films can be controlled. This manuscript reviews the development of the emulsion-based RIR-MAPLE technique and presents new evidence of its applicability for the deposition of conjugated polymer-based optoelectronic devices; namely, hole drift mobility measurements for films deposited by RIR-MAPLE in comparison to traditional solution-based techniques and the demonstration of a multi-layer conjugated polymer optical heterostructure.

2 Review of novel emulsion-based RIR-MAPLE for conjugated polymer deposition

An important aspect of the emulsion-based RIR-MAPLE technique is that it enables selection of evaporative or ablative deposition by controlling the laser-target interaction [33]. Namely, the depth of the laser-target interaction volume (and the corresponding laser energy density) is determined by the absorption of laser energy in the target, which has an enormous impact on the properties of the deposited films. Evaporative deposition (more vaporous ejecta) occurs when the skin-depth of the target to the incident laser is extremely shallow such that the high laser energy density therein evaporates the majority of the frozen solvent. Ablative deposition (more liquid ejecta) occurs when the skin-depth of the target to the incident laser is much longer such that the lower energy density in the absorbing volume is not sufficient to completely vaporize the frozen target. Thus, the transition from evaporative to ablative deposition can be controlled by tuning the skin-depth of the frozen target to the incident laser. The novel emulsion target used in RIR-MAPLE provides an efficient technique to control the skin-depth of the frozen target by controlling the hydroxyl bond concentration in the host solvent matrix via tuning of the water (ice) ratio, which resonantly absorbs the laser energy at 2.9 μm. Importantly, the ability to control the extent to which each deposition regime occurs enables tuning of the conjugated polymer thin-film morphology, i.e.,

the surface morphology can be tuned from very rough to very smooth and the internal morphology can be tuned to increase interchain interactions.

The emulsion-based RIR-MAPLE technique was first developed for the controlled deposition of thin films of the conjugated polymers poly[2-methoxy-5-(2′-ethyl-hexyloxy)-1,4-phenylene vinylene] (MEH-PPV) and poly[2-methoxy-5-(2′ethylhexyloxy)-1,4-(1-cyanovinylene) phenylene] (MEH-CN-PPV) [34]. These two polymers were selected because a large body of research exists that evaluates materials properties of PPV-based polymers in order to provide comparison to RIR-MAPLE-deposited films. It is important to note that MEH-PPV and MEH-CN-PPV both lack a hydroxyl bond, so RIR-MAPLE at 2.9 μm should enable evaporative deposition and should not induce photochemical degradation. In addition, MEH-PPV and MEH-CN-PPV have similar solubility characteristics and are typically solution-processed using solvents such as toluene [36], xylene [17], chloroform [16], chlorobenzene [16], and tetrahydrofuran (THF) [17], none of which possess a hydroxyl bond. In fact, phenol is one of the only PPV-polymer compatible solvents that contain a hydroxyl bond for resonant absorption in the host matrix. Unfortunately, at room temperature, phenol is a solid and is significantly less volatile in comparison to other solvents. Therefore, the novel use of the emulsion target, in which the polymer, solvent, and water are combined, enables RIR- MAPLE deposition of these conjugated polymers.

All RIR-MAPLE depositions were performed using a PVD products Nano-PLD MAPLE system with a pulsed 2.9-μm Er:YAG laser manufactured by Big Sky Laser. The laser was operated in free-running mode with a pulse duration of 90 μs. The typical deposition parameters have been described elsewhere [33, 34]. Film surface morphology was characterized by atomic force microscopy (AFM) using a Veeco 3100 Dimension microscope. Film internal morphology (i.e., extent of interchain interactions within the film) was probed by photoluminescence (PL) spectroscopy [13, 37]. The AFM and PL spectroscopy characterizations were conducted for both as-deposited and annealed films in order to identify any changes in morphology as trapped solvent was annealed away [14]. In particular, ablative deposition with more liquid ejecta results in greater solvent contamination of the substrate. Therefore, when deposited films are annealed to remove trapped solvents, a greater change in the thin-film properties (i.e. surface roughness and PL spectrum) is expected for ablative deposition than for evaporative deposition (with more vaporous ejecta). In this way, the nature of the laser-target interaction for emulsion-based RIR-MAPLE was confirmed and the approach for controlling surface and internal morphologies of conjugated polymer thin films was elucidated.

Film surface roughness is an important figure of merit [38, 39] because smoother films provide more control of film thickness and enhance the quality of the polymer/metal contact interface in devices. In this vein, recent studies have investigated the impact of solvent quality [39] and laser fluence [40] on the surface roughness of MAPLE-deposited films. The surface morphology, represented by the root-mean-squared (RMS) surface roughness, of pre- and post-annealed MEH-CN-PPV thin films deposited by emulsion-based RIR-MAPLE is summarized in Fig. 1 as a function of the hydroxyl bond concentration, which is determined by the phenol:ice target ratio [33]. As demonstrated by these data, as the hydroxyl bond concentration was increased in the target matrix (by increasing the ice content in the target), the subsequent film became smoother. In addition, as the annealing time increased, the RMS surface roughness decreased due to film repair by the escape of trapped solvent [13, 41]. The variation in RMS surface roughness with annealing time was much larger for low hydroxyl bond concentration (low energy density resulting in significant solvent contamination) than for high hydroxyl bond concentration (high energy density resulting in less solvent contamination) because more drastic smoothing occurred for a higher level of solvent contamination [13]. Therefore, the extent to which ablative deposition (low hydroxyl bond concentration) or evaporative deposition (high hydroxyl bond concentration) is achieved by RIR-MAPLE can be controlled by the emulsion target, and such control has a direct effect on the surface roughness of the deposited conjugated polymer thin films. The smoothest film achieved to date using emulsion-based RIR-MAPLE was for a target of 0.25 wt% MEH-PPV in an emulsified 50% phenol:50% water host matrix [34]. As shown in the AFM images of Fig. 2, the resultant film was nearly featureless and the measured RMS surface roughness was 0.3 nm, which is comparable to the smoothest polymer films reported in literature [10]. MAPLE-deposited polymer film roughness reported in literature (not using the emulsion technique) has ranged from 80 nm [39] to 25 nm [42].

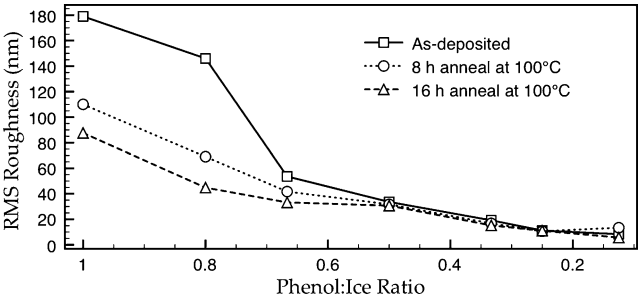

Fig. 1 RMS surface roughness of pre- and post-annealed RIR-MAPLE-deposited MEH-CN-PPV films as a function of increasing hydroxyl bond concentration in the target matrix (phenol:ice ratio)

PL spectroscopy can be used as a tool to elucidate internal polymer chain morphology [13, 14]; specifically, interchain interaction among multiple polymer chains, which is

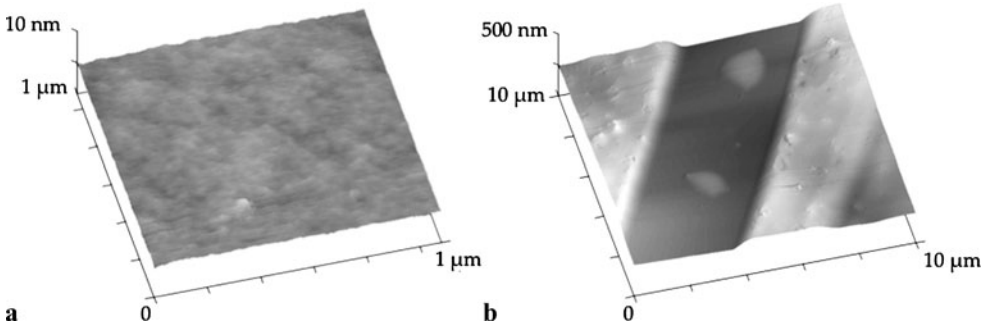

Fig. 2 (**a**) AFM image of a film deposited using 0.25-wt% MEH-PPV in a 50% phenol:50% water emulsified host matrix. (**b**) AFM image of the same film with a portion of the polymer removed to demonstrate film uniformity and thickness (100 nm)

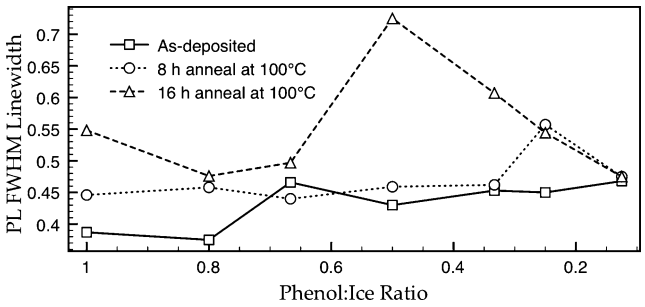

Fig. 3 PL spectra FWHM linewidth of pre- and post-annealed RIR-MAPLE-deposited MEH-CN-PPV films as a function of increasing hydroxyl bond concentration in the target matrix (phenol:ice ratio)

one of the most significant parameters influencing optoelectronic device performance. In a relaxed and isolated conjugated polymer chain, the resultant PL spectrum consists of a single discrete peak with a narrow full width at half maximum (FWHM) linewidth that corresponds to the HOMO-LUMO bandgap, which is an intrachain characteristic. In films with a low density of conformational defects, polymer chains pack together more closely and increase the interchain interaction, which leads to the following changes in the PL spectrum: (i) the conjugated polymer HOMO-LUMO bandgap peak is quenched, (ii) lower energy interchain recombination peaks increase in intensity, and (iii) the FWHM linewidth of the entire PL spectrum increases due to the contribution of the lower energy, interchain recombination peaks [13, 37, 43]. In films with a high density of conformational defects, the interchain interaction is suppressed such that the FWHM linewidth of the entire PL spectrum does not change appreciably due to the absence of lower energy interchain exciton recombination peaks [13]. Thus, the FWHM linewidth of PL spectra indicates the extent to which interchain interactions occur in polymer films.

The measured PL spectra of MEH-CN-PPV thin films deposited by emulsion-based RIR-MAPLE provide evidence for the ability to control the internal morphology of conjugated polymer thin films. As shown in Fig. 3, the PL FWHM linewidth of the entire spectrum increased with increasing hydroxyl bond concentration, indicating that the interchain interaction increased as well. Similarly, the PL FWHM linewidth increased with increasing annealing time, indicating more interchain interaction due to film repair as trapped solvent escaped. It is important to note that for the highest hydroxyl bond concentration, the PL FWHM linewidth exhibited no discernable change with annealing time. This behavior is consistent with the measured RMS surface roughness in that evaporative deposition occurred for the high hydroxyl bond concentration, resulting in minimized solvent contamination of the film. As a result, the interchain interaction did not change appreciably with annealing. Therefore, the extent to which ablative or evaporative RIR-MAPLE deposition occurs depends on the hydroxyl bond concentration in the emulsion target, and such control has a direct effect on the internal morphology (interchain interaction) of the conjugated polymer films.

FTIR absorbance spectroscopy has been conducted in order to ascertain the presence of photochemical polymer degradation of MAPLE-deposited films [28, 30], and previous work demonstrated that the emulsion-based RIR-MAPLE technique does not induce any appreciable photochemical degradation of conjugated polymers [34]. Importantly, a series of papers have demonstrated that even when photochemical degradation is not observed by FTIR absorbance or nuclear magnetic resonance spectroscopy measurements, structural degradation of polymers can occur due to MAPLE and pulsed laser deposition [27, 40, 44]. The extent of structural degradation is determined by measuring the polymer molecular weight using gel permeation chromatography (GPC). Therefore, the molecular weight of conjugated polymer films deposited using the emulsion-based RIR-MAPLE technique was measured by GPC and compared to the as-synthesized molecular weight in order to determine the extent of structural degradation [45]. In addition to MEH-PPV, for this study, emulsion-based RIR-MAPLE was extended to include deposition of poly(3-hexylthiophene) (P3HT), which is an important material for bulk heterojunction solar cells [46–50], and poly(methyl methacrylate) (PMMA), which serves as a standard reference.

The RIR-MAPLE parameters were standardized across depositions to the following values: a target-to-substrate distance of 70 mm; an ambient chamber pressure of 1.33×10^{-4}–1.33×10^{-2} Pa; and a substrate temperature of

4°C. The targets consisted of emulsions of multiple solvents: MEH-PPV was prepared as a 1 wt% solution in toluene:phenol:water; PMMA was prepared as a 1 wt% solution in trichloroethylene (TCE):benzyl alcohol (BnOH): water; and P3HT was prepared as a 1 wt% solution in TCE:phenol:water. The polymer films were deposited onto standard soda-lime glass slides, and subsequently dissolved in tetrahydrofuran (THF), which served as the liquid phase for the GPC analysis in a PLgel, 5-µm, 10^4-Å column from Agilent Technologies. This separation column is appropriate for molecular weights between 4 kDa and 1 MDa, which provided the limits for the as-synthesized molecular weights of the chosen polymers: 245 kDa for MEH-PPV, 43 kDa for P3HT, and 10 kDa and 100 kDa for PMMA. GPC analysis was conducted using an Optilab DSP Interferometric Refractometer and a Dawn Enhanced Optical System, both from Wyatt Technology. Figure 4 shows the measured weight-averaged molecular weights for RIR-MAPLE-deposited MEH-PPV, P3HT, and PMMA, as well as values obtained from literature for other polymers deposited by variations of PLD and MAPLE. In Fig. 4, the weight-averaged molecular weight of deposited films is plotted as a function of the corresponding native molecular weight for the as-synthesized polymer, both of which were measured using GPC. Thus, the diagonal line represents no change in the molecular weight after the deposition process, while data points beneath the line to the lower right represent some reduction in molecular weight indicative of structural degradation, and data points above the line to the upper left represent some increase in molecular weight. All of the PLD films reviewed from literature exhibited significant structural degradation, regardless of laser wavelength, because the solid polymer target absorbs laser energy for deposition. UV-PLD induced a 92% decrease in molecular weight [40], while RIR-PLD induced a molecular weight decrease ranging from 59–63% [51]. UV-MAPLE films also exhibited structural degradation because both the solvent and the polymer absorb laser energy. The damage tended to be more severe at the upper end of the molecular weight scale: a 68–74% decrease was observed for PLGA and [Ru(bpyPMMA$_2$)$_3$]-(PF$_6$)$_2$ with native weights of 33 kDa and 99 kDa, respectively [27, 40], whereas a 5–23% decrease was observed for PEG and PMMA with native molecular weights of 1.4 kDa and 13.9 kDa, respectively [51, 52]. Importantly, the emulsion-based RIR-MAPLE depositions for P3HT and PMMA exhibited no structural degradation because the emulsion matrix absorbs the laser energy. In the case of RIR-MAPLE-deposited MEH-PPV, a 46–50% decrease in molecular weight was observed; however, it is known that PPV-based polymers are sensitive to photo-oxidation that results in chain scission [53]. This mechanism could be responsible for the observed structural degradation. In addition, it is important to note that the native molecular weight for MEH-PPV was higher than any of the other polymers shown. Therefore, some inherent limit due to molecular weight could exist for the emulsion-based RIR-MAPLE process.

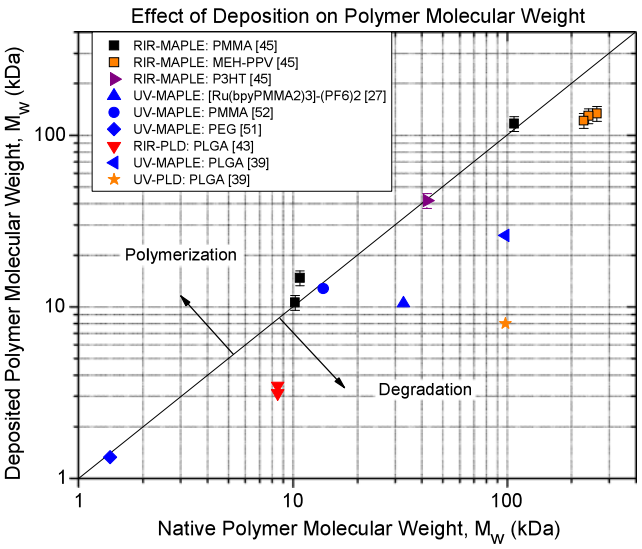

Fig. 4 Deposited vs. native polymer molecular weight. The diagonal line indicates no change in molecular weight. Structural degradation is indicated below the diagonal line

3 Comparison of emulsion-based RIR-MAPLE to spin-cast and drop-cast deposition of conjugated polymers: hole drift mobility

The review of previous work has demonstrated that the emulsion-based RIR-MAPLE technique can deposit polymer thin films with controlled surface morphology, controlled internal morphology, and little to no structural degradation, depending on the specific polymer deposited. The applicability of emulsion-based RIR-MAPLE to conjugated polymer-based optoelectronic devices is now demonstrated by considering charge transport. In conjugated polymers, charge conduction occurs through two mechanisms: intrachain transport and interchain hopping conduction. Intrachain transport occurs when carriers conduct along the backbone of the conjugated polymer. In contrast, interchain hopping conduction occurs when carriers hop from chain to chain. Therefore, it is important to note that the observed structural degradation of MEH-PPV due to emulsion-based RIR-MAPLE deposition should impact intrachain transport along the polymer backbone but should not impact interchain hopping conduction. Importantly, interchain hopping conduction dominates charge transport in conjugated polymer thin films [13]. As a result, charge transport is strongly dependent on the internal morphology of the polymer film and is improved by increased interchain interactions [13, 21, 54, 55].

One useful technique to characterize the level of interchain hopping conduction in a conjugated polymer thin film is to measure the hole drift mobility by time-of-flight (TOF) photoconductivity measurements [54]. As such, the charge transport of RIR-MAPLE-deposited MEH-PPV thin films was characterized and compared to solution-based deposition techniques, namely spin-casting and drop-casting. Extensive work has been conducted to investigate hole mobility in MEH-PPV as a function of deposition technique [21, 54–57]. The internal morphologies of spin-cast and drop-cast MEH-PPV films are different, which accounts for differences in the measured hole drift mobility [57]. Spin-cast films have many in-plane conformational defects due to the centripetal force of the spin-coater, and these defects create large domains of empty space that reduces interchain interaction [21, 54, 57]. In contrast, drop-cast films have fewer conformational defects such that chains are more relaxed, with more interchain interaction [21, 55, 57].

Thus, hole drift mobility measurements were conducted by the TOF method for spin-cast, drop-cast, and RIR-MAPLE-deposited films. The TOF mobility measurement is briefly described as follows. A nanosecond pulsed laser with a wavelength that is readily absorbed by the sample under test (532 nm in the case of MEH-PPV) is directed normally onto a device consisting of a transparent top contact (indium tin oxide—ITO), the active layer under test (MEH-PPV), and a bottom ohmic contact (aluminum). The MEH-PPV active layer absorbs the incident laser radiation and generates excitons, which are immediately dissociated into free carriers near the interface of the active layer and the transparent contact. An applied bias voltage creates an electric field that sweeps holes to the aluminum contact, whereas the electrons are immediately collected by the transparent electrode. The carriers that are swept to the aluminum contact produce a transient photocurrent in a series connected resistor, the decay of which can be analyzed to find the transit time, τ. This transit time represents the amount of time required for holes to traverse the distance from contact to contact. The peak in the measured transient photocurrent decay indicates the transit time, which can then be used to calculate the hole drift mobility:

$$\mu_{\text{drift}} = \frac{d}{E\tau} \tag{1}$$

where d is the film thickness and E is the applied electric field.

Temperature- and electric field-dependent TOF hole drift mobility measurements were conducted for spin-cast, drop-cast, and RIR-MAPLE-deposited films in order to verify that the measured mobility displayed the expected behavior, i.e. the mobility should increase with increasing temperature and with increasing applied electric field. The spin-cast film was prepared by spinning 22 layers of a 1-wt% MEH-PPV-toluene solution onto an ITO substrate to a final thickness

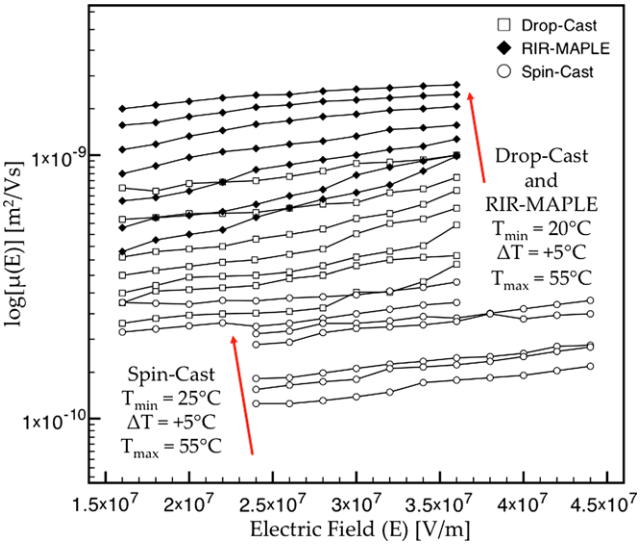

Fig. 5 Hole drift mobility vs. temperature and electric field for spin–cast (*circles*), drop-cast (*squares*), and RIR-MAPLE-deposited (*diamonds*) MEH-PPV thin films. As temperature and electric field are increased, the hole drift mobilties of all of the films increase, and the deposition techniques can be ranked in terms of hole drift mobility as RIR-MAPLE > drop-cast > spin-cast

of approximately 6.5 ± 0.1 μm. The drop-cast film was prepared by drop-casting a 1-wt% MEH-PPV-toluene solution in a toluene-rich atmosphere to a final thickness of approximately 6.5 ± 0.1 μm. The RIR-MAPLE-deposited film was prepared using a target of 1-wt% MEH-PPV in a 1 : 1 : 4, phenol:toluene:deionized water emulsion, a substrate temperature of 25°C, growth pressure of 1.33×10^{-4} Pa, laser fluence of 2 J/cm^2, and substrate-to-target distance of 5 cm such that a final thickness of 6.5 ± 0.1 μm was achieved. During the TOF measurements, the film temperatures were maintained using an ITO substrate heater, all biases were applied using a Keithley E3612A 120 V power supply, and all photocurrent transients were measured across a 100-kΩ resistor using a Tektronix 2024 200-MHz oscilloscope.

The hole drift mobilities (determined using (1)) are shown in Fig. 5 as a function of the applied electric field for each measurement temperature, which ranges from 20°C to 55°C in increments of 5°C. The resultant hole drift mobilities demonstrate that RIR-MAPLE deposition yields the highest hole drift mobility ($\sim 6.0 \times 10^{-10}$ m^2/Vs at 25°C and 2.5×10^7 V/m), whereas drop-cast deposition ($\sim 2.5 \times 10^{-10}$ m^2/Vs at 25°C and 2.5×10^7 V/m) and spin-cast deposition ($\sim 1.1 \times 10^{-10}$ m^2/Vs at 25°C and 2.5×10^7 V/m) yield lower hole drift mobility values. This analysis confirms that RIR-MAPLE-deposited MEH-PPV films exhibit enhanced hole transport properties in comparison to spin-cast and drop-cast films. These findings demonstrate that RIR-MAPLE has an obvious advantage in terms of interchain interaction in conjugated polymer films, which

should prove advantageous to enhancing the performance of conjugated polymer-based optoelectronic devices.

4 Demonstration of multi-layer polymer deposition by emulsion-based RIR-MAPLE

Another important advantage of the emulsion-based RIR-MAPLE technique is now demonstrated, namely the ability to deposit polymer-based, multi-layer films, which are especially useful for the fabrication of optical heterostructures. To date, conjugated polymer-based optoelectronic devices using multi-layer structures have been achieved using materials with different solubility characteristics [58] or a combination of solution and sol-gel processing [8]; however, many desirable multi-layer structures are difficult to achieve using traditional solution processing techniques because the constituent layers have similar solubility characteristics. For example, the fabrication of a polymer-based, one-dimensional (1D) distributed Bragg reflector (DBR) faces the important challenge that the selection of polymers (and corresponding refractive indices) is often limited by solubility characteristics as many technologically attractive polymers are soluble in aromatic and/or chlorinated solvents. Furthermore, the solvents could damage the active layer of any conjugated polymer-based optoelectronic device if its solubility is similar to that of the DBR cladding layers. In contrast, emulsion-based RIR-MAPLE has the unique capability to enable multi-layer heterostructures of polymers with similar solubility characteristics because the evaporative growth regime significantly reduces substrate exposure to the host solvent. Therefore, as a demonstration, the characterization of a polymer-based DBR fabricated using emulsion-based RIR-MAPLE is presented.

Emulsion-based RIR-MAPLE was used to fabricate a 1D DBR using P3HT and PMMA, which were selected as the constituent materials because they have significantly different indices of refraction (2.0 [59] and 1.49 [60], respectively) and similar solubility characteristics (soluble in chlorinated and aromatic solvents). The refractive indices of RIR-MAPLE-deposited P3HT and PMMA thin films were verified by spectroscopic ellipsometry to match the values quoted in literature. The DBR structure was designed to have peak reflectivity at 1127 nm (1.1 eV) because this wavelength corresponds to the spectral response of a conjugated polymer-based infrared photodetector [61]. Thus, the simulated design comprises eight periods of P3HT and PMMA, wherein the thickness of each polymer film is 140.9 nm and 189.2 nm, respectively. The reflectivity spectrum for the simulated design is shown in Fig. 6.

Based on this design, RIR-MAPLE was used to deposit an eight-period PMMA-P3HT DBR structure on a glass substrate, with PMMA as the first deposition layer. The P3HT and PMMA polymers were dissolved into chloroform and toluene, respectively, at 0.5 wt%, and the separate emulsion targets comprised phenol and water. AFM microscopy was used to calibrate the respective growth rates of P3HT and PMMA (0.57 nm/min and 0.56 nm/min) by dividing the thickness of a calibration film by the deposition time. It is important to note that these growth rates were selected in order to obtain sufficiently smooth films, yet minimize the total growth time for the DBR structure. Figure 7 shows an AFM image of the surface morphology for the PMMA calibration film. The RMS surface roughness for the P3HT and PMMA calibration films were 13 nm and 8 nm, respectively.

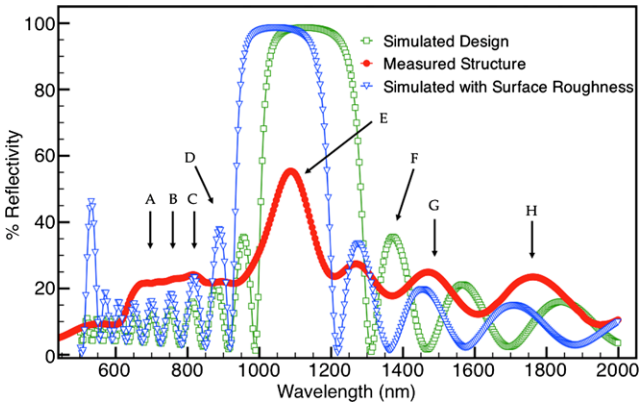

Fig. 6 Comparison of simulated reflectivity spectra and measured reflectivity spectrum of the RIR-MAPLE-deposited DBR. The measured reflectivity peaks are offset from the simulated design due to slight variations in film thickness resulting from surface roughness. When film thickness variability is incorporated into the simulation, the simulated spectrum blue shifts and better matches the measured spectrum

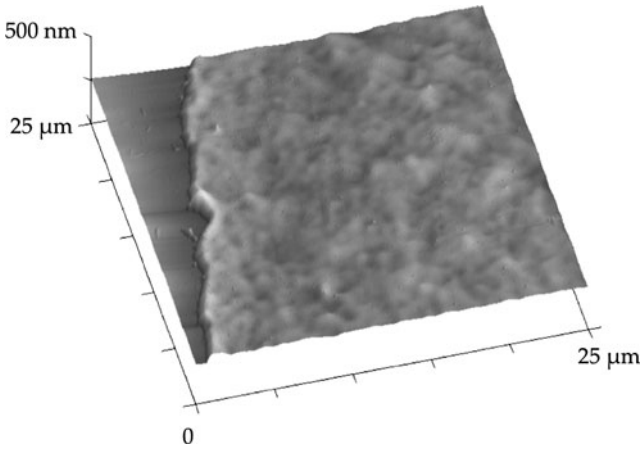

Fig. 7 AFM image of a PMMA film deposited by RIR-MAPLE for the DBR structure. This film is representative of both P3HT and PMMA films and has an RMS surface roughness of approximately 8 nm (13 nm for P3HT). The measured RMS surface roughness of the depicted area is representative of the entire surface of the substrate. The dark area is where the film has been removed to show the substrate and indicate film thickness

The reflectivity of the RIR-MAPLE-deposited DBR structure was measured using an Ocean Optics UV-VIS reflectometer, and the resultant spectrum is shown in Fig. 6, wherein several reflectivity peaks are observed. In the visible spectrum, the reflectivity peaks from 400 to 900 nm (Peaks A-D) are difficult to observe in the measured spectrum because this wavelength range contains the primary HOMO-LUMO absorption band of the P3HT polymer (450 to 600 nm) [10]. The primary measured reflectivity peak at 1087 nm (Peak E) is very close to the simulated design peak of 1127 nm with an approximate error of 3.62%. The measured peak reflectivity at 1087 nm is 55.4%, which is much less than the peak reflectivity predicted by the simulated design. This significant reduction in peak reflectivity for the measured DBR is most likely due to the polymer film surface roughness, that is, slight thickness variations across the constituent films effectively reduces the reflectivity due to light scattering and decreased constructive interference [62]. The impact of film surface roughness is also observed by comparing the infrared reflectivity peaks (Peaks F, G, and H) for the measured DBR and the simulated design spectra. Peaks F, G, and H of the measured spectrum exhibit errors of 7.62%, 6.32%, and 4.33%, respectively, compared to the simulated design spectrum. In order to account for this discrepancy, the reflectivity spectrum is simulated by incorporating the measured RMS surface roughness of the P3HT and PMMA films (13 nm and 8 nm, respectively). The resultant simulated reflectivity spectrum accounting for surface roughness is also shown in Fig. 6, and the measured reflectivity spectrum Peaks F, G, and H exhibit much better agreement, with errors of 0.24%, 1.09%, and 3.11%, respectively. Therefore, it is anticipated that further RIR-MAPLE optimization designed to balance surface roughness and growth rates will result in smoother films that yield higher peak reflectivities. In any case, the measured reflectivity spectrum of the polymer-based DBR deposited by RIR-MAPLE demonstrates that a multi-layer structure with sufficient control of film thickness and relatively discrete interfaces has been achieved despite the similar solubility characteristics of the constituent polymers.

5 Conclusions

The novel emulsion target RIR-MAPLE technique has been demonstrated to be a robust and flexible method for the deposition of device quality conjugated polymer thin films and heterostructures. The demonstrated abilities to repeatedly and reliably deposit conjugated polymer films with controlled thickness, surface morphology, and internal morphology; to enhance hole mobility and interchain interaction; and to enable multi-layer deposition of polymers in optical heterostructures, regardless of their solubility characteristics, are difficult to achieve using traditional solution-based deposition. As a result, emulsion-based RIR-MAPLE should enable enhanced performance of existing conjugated polymer-based optoelectronic devices, as well as new conjugated polymer optoelectronic device designs. Importantly, this work helps to transition RIR-MAPLE from being a research topic in its own right toward becoming a more mainstream deposition technique, especially for conjugated polymer- based optoelectronic devices.

Acknowledgements This work was supported in part by the Office of Naval Research under Grant No. N00014-07-1-0799 and Grant No. N00014-10-1-0481, the National Science Foundation under Grant No. 0547273, and the Air Force Office of Scientific Research under Grant No. FA9550-06-1-0482.

References

1. H. Shirakawa, E.J. Louis, A.G. Macdiarmid, C.K. Chiang, A.J. Heeger, J. Chem. Soc., Chem. Commun. **16**, 578 (1977)
2. R. McNeill, J.H. Wardlaw, D.E. Weiss, Aust. J. Chem. **16**(663), 1056 (1963)
3. S.A. McDonald, G. Konstantatos, S. Zhang, P.W. Cyr, E.J.D. Klem, L. Levina, E.H. Sargent, Nat. Mater. **4**(2), 138 (2005)
4. A.D. Stiff-Roberts, J. Nanophotonics **3**, 031607 (2009)
5. M. Gaal, C. Cadermaier, H. Plank, E. Moderegger, A. Pogantsch, G. Leising, E.J. List, Adv. Mater. **15**(14), 1165 (2003)
6. J.H. Burroughes, D.D.C. Bradley, A.R. Brown, R.N. Marks, K. Mackay, R.H. Friend, P.L. Burns, A.B. Holmes, Nature **347**, 539 (1990)
7. G. He, J. Liu, Y. Li, Y. Yang, Appl. Phys. Lett. **80**(11), 1891 (2002)
8. J.Y. Kim, K. Lee, N.E. Coates, D. Moses, T. Nguyen, M. Dante, A.J. Heeger, Science **317**(5835), 222 (2007)
9. J.Y. Kim, S.H. Kim, H.H. Lee, K. Lee, W. Ma, X. Gong, A.J. Heeger, Adv. Mater. **18**(5), 572 (2006)
10. S. Günes, H. Neugebauer, N.S. Sariciftci, Chem. Rev. **107**, 1324 (2007)
11. M. Reyes-Reyes, K. Kim, D.L. Carroll, Appl. Phys. Lett. **87**, 083506 (2005)
12. H. Sirringhaus, N. Tessler, R.H. Friend, Science **280**(5370), 1741 (1998)
13. B.J. Schwartz, Annu. Rev. Phys. Chem. **54**, 141 (2003)
14. S.A. Arnautov, E.M. Nechvolodova, A.A. Bakulin, S.G. Elizarov, A.N. Khodarev, D.S. Martyanov, D.Y. Paraschuk, Synth. Met. **147**(1), 287 (2004)
15. T.Q. Nguyen, R.C. Kwong, M.E. Thompson, B.J. Schwartz, Appl. Phys. Lett. **76**(17), 2454 (2000)
16. T.Q. Nguyen, I.B. Martini, J. Liu, B.J. Schwartz, J. Phys. Chem. B **104**(2), 237 (2000)
17. Y. Shi, J. Liu, Y. Yang, J. Appl. Phys. **87**(9), 4254 (2000)
18. X. Li, F. Cacialli, R. Cervini, A.B. Holmes, S.C. Moratti, A.C. Grimsdale, R.H. Friend, Synth. Met. **84**(1), 159 (1997)
19. H. Sirringhaus, T. Kawase, R.H. Friend, T. Shimoda, M. Inbasekaran, W. Wu, E.P. Woo, Science **290**, 2123 (2000)
20. R. Saf, M. Goriup, T. Steindl, T.E. Hamedinger, D. Sandholzer, G. Hayn, Nat. Mater. **3**(5), 323 (2004)
21. A.R. Inigo, C.C. Chang, W. Fann, J.D. White, Y.S. Huang, U.S. Jeng, H.S. Sheu, K.Y. Peng, S.A. Chen, Adv. Mater. **17**(15), 1835 (2005)

22. W. Ma, P.K. Iyer, X. Gong, B. Liu, D. Moses, G.C. Bazan, A.J. Heeger, Adv. Mater. **17**(3), 274 (2005)
23. A. Piqué, R.A. McGill, D.B. Chrisey, D. Leonhardt, T.E. Msina, B.J. Spargo, J.H. Callahan, R.W. Vachet, R. Chung, M.A. Bucaro, Thin Solid Films **355**(1), 536 (1999)
24. L. Zhigilei, E. Leveugle, J. Appl. Phys. **102**(7), 074914 (2007)
25. E. Leveugle, L.V. Zhigilei, A. Sellinger, J.M. Fitz-Gerald, Appl. Surf. Sci. **253**, 6456 (2007)
26. R.D. Torres, S.L. Johnson, R.F. Haglund, J.H. Hwang, P.L. Burn, P.H. Holloway, Crit. Rev. Solid State Mater. Sci. **36**(1), 16 (2011)
27. J.M. Fitz-Gerald, G. Jennings, R. Johnson, C.L. Fraser, Appl. Phys. A **80**(5), 1109 (2005)
28. B. Toftmann, M.R. Papantonakis, R.C.Y. Auyeung, W. Kim, S.M. O'Malley, D.M. Bubb, J.S. Horwitz, J. Schou, P.M. Johansen, R.E. Haglund, Thin Solid Films **453–454**, 177 (2004)
29. D.B. Chrisey, A. Piqué, A. McGill, J.S. Horwitz, B.R. Ringeisen, Chem. Rev. **103**, 553 (2003)
30. P.R. Griffiths, *Fourier Transform Infrared Spectrometry Chemical Analysis* (Wiley-Interscience, New York, 2007)
31. D.M. Bubb, S.M. O'Malley, C. Antonacci, D. Simonson, R.A. McGill, J. Appl. Phys. **95**(4), 2175 (2004)
32. R. Pate, K.R. Lantz, A. Dhawan, T. Vo-Dinh, A.D. Stiff-Roberts, AIP Conf. Proc. **1278**, 813 (2010). (International Symposium on High Power Laser Ablation)
33. R. Pate, A.D. Stiff-Roberts, Chem. Phys. Lett. **477**(4–6), 406 (2009)
34. R. Pate, K.R. Lantz, A.D. Stiff-Roberts, IEEE J. Quantum Electron. **14**(4), 1022 (2008)
35. R. Pate, K.R. Lantz, A.D. Stiff-Roberts, Thin Solid Films **517**(24), 6798 (2009)
36. S. Shaked, S. Tal, Y. Roichman, A. Razin, S. Xiao, Y. Eichen, N. Tessler, Adv. Mater. **15**(11), 913 (2003)
37. F. Kong, S.Y. Zhang, C.Z. Yang, R.K. Yuan, Mater. Lett. **60**(29), 3887 (2006)
38. D.M. Bubb, A.O. Sezer, J. Gripenburg, B. Collins, E. Brookes, Appl. Surf. Sci. **253**(15), 6465 (2007)
39. D.M. Bubb, M. Papantonakis, B. Collins, E. Brookes, J. Wood, U. Gurudas, Chem. Phys. Lett. **448**(4–6), 194 (2007)
40. A.L. Mercado, C.E. Allmond, J.G. Hoekstra, J.M. Fitz-Gerald, Appl. Phys. A **81**(3), 591 (2005)
41. K.E. Strawhecker, S.K. Kumar, J.F. Douglas, K. Alamgir, Macromolecules **34**(14), 4669 (2001)
42. D.M. Bubb, J. Corgan, S.Y. Yi, M. Khan, L. Hughes, U. Gurudas, M. Papantonakis, R.A. McGill, Appl. Phys. A **100**, 523 (2010)
43. C. Wu, C. Hsieh, D. Chen, S. Chang, K. Chen, Synth. Met. **155**(3), 618 (2005)
44. D.M. Bubb, B. Toftmann, J.R.F. Haglund, J.S. Horwitz, M.R. Papantonakis, R.A. McGill, P.W. Wu, D.B. Chrisey, Appl. Phys. A **74**(1), 123 (2002)
45. R. McCormick, A.D. Stiff-Roberts, J. Lenhardt, Presented at the Materials Research Society Fall Meeting, Boston, MA, 2010 (unpublished)
46. J. Ouyang, Y. Xia, Sol. Energy Mater. Sol. Cells **93**, 1592 (2009)
47. R. Mauer, M. Kastler, F. Laquai, Adv. Funct. Mater. **20**(13), 2085 (2010)
48. R.A. Marsh, J.M. Hodgkiss, S. Albert-Seifried, R.H. Friend, Nano Lett. **10**(3), 923 (2010)
49. S. Lilliu, T. Agostinelli, E. Pires, M. Hampton, J. Nelson, J.E. Macdonald, Macromolecules **44**(8), 2725 (2011)
50. S.P. Speakman, G.G. Rozenberg, K.J. Clay, W.I. Milne, A. Ille, I.A. Gardner, E. Bresler, J.H.G. Steinke, Org. Electron. **2**, 65 (2001)
51. D.M. Bubb, P.K. Wu, J.S. Horwitz, J.H. Callahan, M. Galicia, A. Vertes, R.A. McGill, E.J. Houser, B.R. Ringeisen, D.B. Chrisey, J. Appl. Phys. **91**(4), 2055 (2002)
52. A.T. Sellinger, A.H. Martin, J.M. Fitz-Gerald, Thin Solid Films **516**(18), 6033 (2008)
53. M. Jørgensen, K. Norrman, F.C. Krebs, Sol. Energy Mater. Sol. Cells **92**(7), 686 (2008)
54. A.R. Inigo, H.C. Chiu, W. Fann, Y.S. Huang, U.S. Jeng, T.S. Lin, C.H. Hsu, K.Y. Peng, S.A. Chen, Phys. Rev. B **69**(7), 075201 (2004)
55. Y.F. Huang, A.R. Inigo, C.C. Chang, K.C. Li, C.F. Liang, C.W. Chang, T.S. Lim, S.H. Chen, J.D. White, U.S. Jeng, A.C. Su, Y.S. Huang, K.Y. Peng, S.A. Chen, W.W. Pai, C.H. Lin, A.R. Tameev, S.V. Novikov, A.V. Vannikov, W.S. Fann, Adv. Funct. Mater. **17**, 2902 (2007)
56. M.H. Li, H.L. Chen, Y.F. Huang, W.T. Chuang, Y.R. Chen, H.S. Tsai, O.A. Semenikhin, J.D. White, Chem. Phys. Lett. **505**, 100 (2011)
57. A.R. Inigo, Y.F. Huang, J.D. White, Y.S. Huang, W.S. Fann, K.Y. Peng, S.A. Chen, J. Chin. Chem. Soc. **57**, 459 (2010)
58. T. Komikado, S. Yoshida, S. Umegaki, Appl. Phys. Lett. **89**, 061123 (2006)
59. S. Marchant, W.R.E. Brakenbury, J. Horder, P.J.S. Foot, J. Mater. Sci. Lett. **12**, 1154 (1993)
60. J. Dlutowski, A.M. Cardenas-Valencia, D. Fries, L. Langebrake, J. Chem. Educ. **83**(12), 1867 (2006)
61. S.H. Im, J.A. Chang, S.W. Kim, S.W. Kim, S.I. Seok, Org. Electron. **11**, 696 (2010)
62. K.D. Singer, T. Kazmierczak, J. Lott, H. Song, Y. Wu, J. Andrews, E. Baer, A. Hiltner, C. Weder, Opt. Express **16**(14), 10358 (2008)